Journal of Power Sources 224 (2013) 72–79

Contents lists available at SciVerse ScienceDirect

Journal of Power Sources

journal homepage: www.elsevier.com/locate/jpowsour

Lithium intercalation in nanostructured thin films of a mixed-valence layered vanadium oxide using an ionic liquid electrolyte

Tânia M. Benedetti [a], Emily Redston [a,1], Willian G. Menezes [b], Dayane M. Reis [b], Jaísa F. Soares [b], Aldo J.G. Zarbin [b], Roberto M. Torresi [a,*]

[a] Instituto de Química, Universidade de São Paulo (USP), CP 26077, 05513-970 São Paulo-SP, Brazil
[b] Departamento de Química, Universidade Federal do Paraná (UFPR), CP 19081, 81530-900 Curitiba-PR, Brazil

HIGHLIGHTS

- Thin films of vanadium oxide were prepared by layer-by-layer deposition.
- Film growth were analyzed by kinetic and isothermal approaches.
- Good initial capacity were obtained in organic solvent and ionic liquid electrolytes.
- Better capacity retention was obtained in ionic liquid electrolyte.

ARTICLE INFO

Article history:
Received 17 July 2012
Received in revised form
13 September 2012
Accepted 15 September 2012
Available online 3 October 2012

Keywords:
Lithium microbatteries
Vanadium oxide
Ionic liquids
Layer-by-layer
Adsorption isotherm
Adsorption kinetic

ABSTRACT

Nanostructured thin films of a mixed-valence, layered vanadium oxide were prepared using layer-by-layer deposition. The thin films were characterized by electronic (UV–vis) spectroscopy, quartz crystal microbalance, profilometry and scanning electron microscopy techniques. The highest charge capacity was obtained for films that consisted of 25 bilayers. The electrochemical characterization of the films was performed in conventional organic solvent and ionic liquid (IL) based electrolytes. The results revealed better performance, in terms of stability during consecutive charge/discharge cycles, when ILs were employed. This can be attributed to several factors, including reduced mechanical stress caused by insertion of more than 1 mol of Li^+ per mol of V^{5+} in the film structure, decrease of crystallinity in the electrode material during the first few charge/discharge cycles and/or formation of a more compatible SEI. Nanostructured thin films of layered vanadium oxide prepared using layer-by-layer deposition showed potential for applications in lithium microbatteries.

1. Introduction

Due to their high voltage and energy, Li-ion batteries are the most commonly used power supplies for portable electronic equipment such as laptops and cell phones [1]. The expansion of applications in new fields such as microelectronics, telecommunication, medical implants, the military industry and radio frequency identification (RFID), have motivated the development of ever-smaller devices for energy storage and conversion, the so-called microbatteries.

Lithium microbatteries are solid state systems in which components are stacked in a cell that is few micrometers thick [2]. Because of these size constraints, many studies have focused on the development of thin films as electrode materials [3]. However, miniaturization results in poor charge capacity when the films are prepared through conventional deposition techniques, where the amount of electroactive material available for Li^+ intercalation is low. To obtain a thin film with suitable charge capacity, it is necessary to develop materials with higher surface areas, which can be accomplished with nanostructured architectures. Several publications have reported the use of nanostructured films as cathodes for Li-ion batteries [4–13], which showed promising results in this application.

In this work, nanostructured thin films were prepared from nanoparticles of mixed-valence, layered hydrated vanadium oxide, $V_{10}O_{24}\cdot 9H_2O$. Vanadium oxide, together with manganese oxide [14–24], is promising substitutes to the common used $LiCoO_2$,

* Corresponding author. Tel.: +55 11 30919194; fax: +55 11 38155640.
E-mail address: rtorresi@iq.usp.br (R.M. Torresi).
[1] Present address: School of Engineering and Applied Sciences, Harvard University, Cambridge, MA 02138, USA.

0378-7753/$ – see front matter © 2012 Elsevier B.V. All rights reserved.
http://dx.doi.org/10.1016/j.jpowsour.2012.09.058

which presents safety issues and high cost. Particularly, vanadium oxide performance can be improved by the use of hydrated structures, which increase the distance between the oxide layers, facilitating Li^+ intercalation [25].

The nanoparticles were immobilized by the simple and low cost layer-by-layer deposition technique, using polyallylamine (PAH) as the polycation. The protonated amino groups from PAH interact with oxygen atoms from vanadyl groups, shielding the interaction with Li^+, facilitating their diffusion through the film structure [26]. Moreover, the vanadium oxide employed in this study presents an unusual mixed-valence bariandite layered structure as it is possible to observe in a previous contribution from some of us [27] and preliminary studies showed its potential for use as cathode in Li-ion batteries.

Electrochemical characterization was performed in conventional organic solvent- and ionic liquid-based electrolytes. Ionic liquids are salts consisting of voluminous cations and asymmetric anions with delocalized charge distributions, giving rise to liquid substances [28]. Their unique properties, such as high conductivity, negligible volatility/flammability and high chemical and electrochemical stabilities, qualify them as promising alternatives to volatile organic solvents as electrolytes [29,30]. There have been only a few studies of the electrochemical performance of vanadium oxides in ionic liquid-based electrolytes [31–33]; the promising results encouraged additional studies in this field. Besides, the ionic liquid chosen for this study, 1-butyl-2,3-dimethylimidazolium bis(trifluoromethylsulfonyl)imide ([BMMI][Tf_2N]), is stable against metallic lithium [34] allowing the use of this metal as anode.

2. Experimental

2.1. Chemicals

All reactants for thin film preparation and characterization – PAH, mercaptoundecanoic acid (MUA), poly(-diallyldimethylammonium chloride) (PDDA), lithium perchlorate ($LiClO_4$), propylene carbonate (PC) and lithium trifluoromethanesulfonate ($LiCF_3SO_3$) – and for ionic liquid synthesis – 1,2-dimethylimidazole, butyl bromide and lithium bis(trifluoromethanesulfonyl)imide ($LiTf_2N$) – were purchased from Aldrich and used as received. The ionic liquid synthesis was described in previous work [34].

2.2. Instrumental

Suspensions of vanadium oxide nanoparticles (NPs) were prepared with an ultrasonic probe from Sonics-Vibracell. Morphological characterization was carried out by field emission scanning electron microscopy (FESEM) with a Jeol microscope, model JSM-7401F. The film thickness was measured with a Dektak 3 profilometer. Thin film growth was monitored by UV–vis spectroscopy with an HP 8452A instrument and a quartz crystal microbalance (QCM), equipped with a 6 MHz AT-cut overtone polished piezoelectric quartz crystal (Valpey-Fisher) with a diameter of 25 mm and a piezo-active electrode area of 0.31 cm^2 (integral sensitivity factor, $K = 6.45 \times 10^7$ cm^2 Hz g^{-1} [35]). Both sides of the quartz electrode were treated with chromium to improve the adhesion of gold to the quartz. Then, multilayered films were deposited on the quartz/Au electrode. Frequency shifts during film formation were measured with a Stanford Research Systems Model SR620 instrument connected to an oscillating circuit (serial mode) and a microcomputer for data acquisition.

2.3. Layer-by-layer deposition of $V_{10}O_{24}\cdot 9H_2O$ thin films

The NPs were prepared according to a procedure described elsewhere [27]. Briefly, the vanadium(IV) alkoxide precursor, $[V_2(OPr^i)_8]$ (Pr^i = isopropyl) [36], was submitted to sol–gel processing at 55 °C for 50 h, and the product was isolated, washed and dried at 55 °C for 12 h. The NPs were suspended in water by immersing an ultrasonic probe in the suspension; different durations of ultrasonic frequency were tested to obtain the most suitable suspension for preparing the films. Layers were deposited by alternately immersing substrates into NPs suspensions and a 10 mg mL^{-1} aqueous solution of PAH at pH = 3. The immersion times were fixed at 10 min for PAH and defined by UV–vis measurements for NPs suspensions. Two different substrates were used: glass slides coated with indium tin oxide (ITO – resistance below 20 Ω from Delta Technologies) and a quartz crystal (described in Section 2.2), which was pre-treated (12 h in MUA 5 mmol L^{-1} in ethanol, followed by 10 min in PDDA 2 mmol L^{-1} at pH = 12) prior to deposition. The substrate was washed with water and dried with N_2 between depositions. Each sequence (PAH-wash-NPs-wash) produced a bilayer. The UV–vis and QCM methods were used to monitor the growth of bilayers on ITO-coated glass and quartz crystal substrates, respectively. Sauerbrey's equation was used to convert frequency shifts into mass values [37]. The morphology of the thin films was characterized by FESEM, and their thickness was measured by profilometry.

2.4. Electrochemical characterization

Electrochemical characterization was performed under argon atmosphere in a glove box from MBraun with O_2 and H_2O levels below 1 ppm. The chamber was connected to an Autolab potentiostat, model PGSTAT 30. Cyclic and linear voltammetry scans were performed using thin films on ITO substrates. Metallic lithium was used for both counter and reference electrodes. The electrolytes were 0.5 mol L^{-1} $LiClO_4$ solution in PC and 0.03 mol L^{-1} $LiCF_3SO_3$ solution in [BMMI][Tf_2N].

3. Results and discussion

3.1. Layer-by-layer formation of $V_{10}O_{24}\cdot 9H_2O$ thin films

Before LBL techniques were used to deposit NPs, different concentrations of vanadium oxide NPs and various durations of ultrasonic radiation at 15 W were tested. The stability of the resulting suspensions was studied with UV–vis measurements at different times after their preparation. Based on the results, the sonication time was set at 30 min, which yielded stable suspensions at concentrations up to 0.5 g L^{-1}. The deposition of NPs through the LBL deposition did not take place when freshly prepared suspensions were used. Instead, it was possible to deposit growing amounts of NPs, employing the same immersion time, over subsequent days after suspension preparation. Maximum deposition was achieved 20 days after suspensions were prepared. At this point, the suspension is opaque instead of transparent (as observed after they were prepared). According to previous studies, NPs consist of two dimensional superimposed ($300 \times 50 \times 1$) nm layers with bariandite structure. Ultrasonic radiation separates (exfoliates) these layers and forms transparent suspensions of NPs. It is believed that these layers are strongly solvated, and because solvation enthalpy is probably more energetically favorable than the entropic gain due to desolvation [38], deposition does not take place at this point.

However, as long as the layers re-aggregate, the entropic gain contribution becomes more important than the solvation enthalpy

and makes it possible for deposition to occur. The LBL deposition was carried out 20 days after the suspensions were prepared, at the NPs concentrations and immersion times that were optimized with UV–vis measurements. Fig. 1a shows the absorbance of the first layer deposited on an ITO substrate as a function of the immersion time at different NPs suspension concentrations.

The curves revealed that deposition is very fast at the beginning of the experiments (approximately the first 2 min) and tends to reach a plateau after 10 min. The final film absorbance is greater for higher initial NPs suspension concentrations, which can be explained based on the mass gradient pressure that acts as a driving force to transfer species from bulk solution to the surface of substrate. Based on these results, suspension concentration for thin film preparation was set at 0.5 g L^{-1}. Fig. 1b shows the absorbance of films deposited from 0.5 g L^{-1} suspensions over ITO substrates as a function of immersion time for different numbers of bilayers. The data were normalized by the absorbance of the former bilayer. These curves show that deposition over previously deposited material followed the same behavior as for the first layer deposited over the bare substrate. These results also showed that a higher quantity of NPs was deposited with increasing numbers of bilayers, which can be attributed to increasing film roughness. The kinetics of the adsorption process were studied by fitting the absorbance versus time curves with a pseudo-second order kinetic model (equation (1)) [39], which is accepted widely for adsorption reactions [40]:

$$A_{(t)} = \frac{KA_e^2 t}{1 + KA_e t} \quad (1)$$

In (1), $A_{(t)}$ is the absorbance at a given time, t; K is the adsorption kinetics constant and A_e is the absorbance at equilibrium. This model fits the experimental data very well, with $R^2 > 0.95$ for all concentrations and numbers of bilayers. The adsorption followed the same behavior independent of suspension concentration and deposition over a bare substrate or an existing layer. The pseudo-second order model assumes that the rate limiting step is chemisorption, which involves the sharing or exchanging of electrons between the adsorbed species and substrate [41]. In a previous work by Alcantara et al. [42], the deposition of $CoFe_2O_4$/PSS films by LBL was observed to have pseudo first-order behavior. This means that deposition conditions affect deposition mechanism. In fact, in the contribution of Alcantara et al., very low suspension concentrations have been employed (from 2×10^{-5} to 2×10^{-4} g L^{-1}) when compared with the ones from the present work. In the present work, fitting the experimental data with a pseudo first order model resulted in poor fits with low R^2 values.

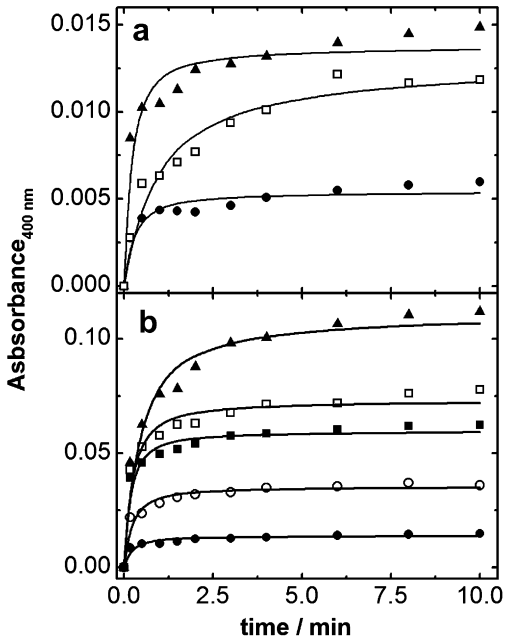

Fig. 1. Normalized absorbance at 400 nm as a function of immersion time on ITO (a) in NP suspensions of different concentrations: 0.025 g L^{-1} (●), 0.25 g L^{-1} (□) and 0.5 g L^{-1} (▲); and (b) 0.5 g L^{-1} suspension and different numbers of bilayers: 1 (●), 10 (○), 18 (■), 26 (□) and 40 (▲) bilayers. Initial absorbances for 1 bilayer: 0.1356; 10 bilayers: 0.2630; 18 bilayers: 0.4616; 26 bilayers: 0.7517; 40 bilayers: 1.1349.

Table 1
Equilibrium constant (K) and equilibrium factor (R_w) calculated from equations (1) and (2), respectively, for the first layer deposited from different suspension concentrations.

NPs suspension [] g L^{-1}	K	q_{eq}	R_w
0.01	13.9	0.005	0.59
0.25	13.1	0.013	0.56
0.5	7.9	0.014	0.49

The equilibrium factor (R_w), which is a measure of how close the system is to equilibrium at a given time, was calculated from equation (2) [40], where t_{ref} is the longest operation time:

$$R_w = \frac{1}{1 + Kq_e t_{ref}} \quad (2)$$

The values of the equilibrium constant (K), adsorbed concentration at equilibrium (q_e) and equilibrium factor (R_w), as functions of suspension concentration and number of bilayers, are listed in Tables 1 and 2, respectively. All R_w values were between 1 and 0.1, which indicated that adsorption is approaching equilibrium at 10 min for all concentrations [40]. Although the equilibrium was not reached at this time, the immersion time was set at 10 min because adsorption was too slow after that time; in fact, R_w only achieves a level below 0.01, in which adsorption is very close to equilibrium, after approximately 16 h of immersion, with no significant improvement in the amount of deposited material.

The calculated values of K and q_e show that at lower concentrations, equilibrium is achieved more rapidly, but less material is deposited at equilibrium. The higher the suspension concentration, the longer is the time required for system to achieve equilibrium and the higher is the amount of deposited material. The effect of this behavior can be observed in the plot of the absorbance at 400 nm (Fig. 2a) and mass of vanadium oxide (Fig. 2b) as function of number of bilayers.

According to Fig. 2, film growth follows exponential behavior for approximately 20 bilayers and tends toward linear growth in the subsequent bilayers. This behavior is in agreement with the kinetic studies: when the first bilayers are formed, the kinetic constant is higher and equilibrium is reached readily; consequently, a larger amount of material is deposited with an increasing number of

Table 2
Equilibrium constant (K) and equilibrium factor (R_w) calculated from equations (1) and (2), respectively, for different bilayers deposited from 0.5 g L^{-1} suspension concentration.

Bilayer	K	q_{eq}	R_w
1	7.9	0.014	0.49
10	2.9	0.03	0.53
18	2.4	0.06	0.41
26	1.4	0.07	0.50
40	0.4	0.11	0.69

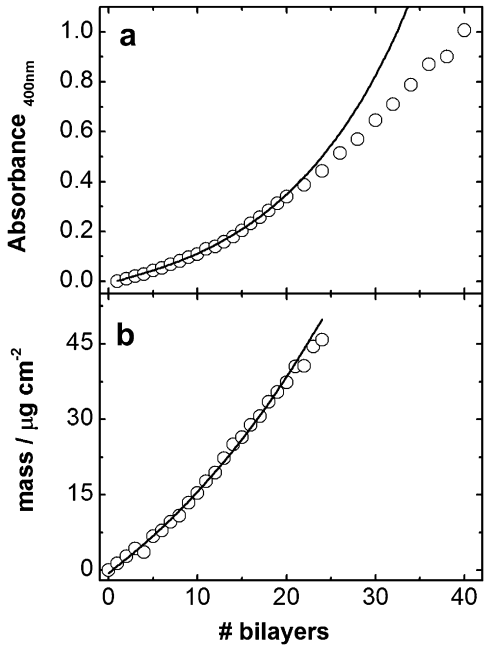

Fig. 2. (a) Absorbance at 400 nm as a function of the number of bilayers. (b) Mass of vanadium oxide deposited as a function of the number of bilayers obtained by QCM. Suspension concentration: 0.5 g L^{-1}.

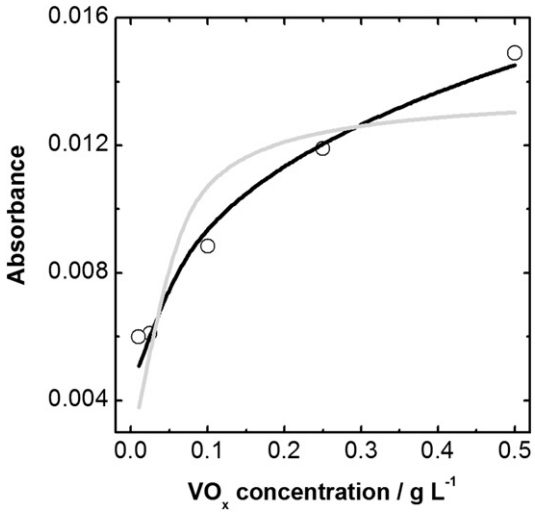

Fig. 3. Fitting of absorbance versus NP suspension concentration. Experimental data (●), fitted with the Freundlich model (black line) and the Langmuir model (gray line).

bilayers. However, after a higher number of bilayers are formed, despite the possibility of depositing a larger amount of NPs, the equilibrium is not reached rapidly, and the rate of deposition decreases. The physical explanation for this behavior comes from the fact that the substrate has low charge density; so that, a lower amount of material is electrostatically "attached" to the substrate and higher amount of "charged sites" are available for deposition of the subsequent layer [38]. This behavior is clearly observed in Fig. 2a and, in spite of the lower number of bilayers employed, the same behavior is observed when film growth is monitored by QCM (Fig. 2b).

To verify the stability of the vanadium oxide film during immersion in PAH solution, UV–vis spectra were also taken after immersion in the polycation (results not shown): absorbance decreases approximately 13% after each immersion in PAH, which means that some of the previously deposited NPs are lost during polycation deposition. Thus, it was not possible to determine the mass by QCM measurements of deposited PAH because the frequency shift before and after immersion in the PAH solution corresponds to the mass of PAH minus the loss of NPs. For calculations of the mass of NPs deposited after each immersion, the 13% loss observed from UV–vis measurements was used and the calculated value is 0.96 μg cm^{-2} (the average value obtained for each NPs bilayer). This value was used for calculations in the electrochemical characterization.

The adsorption mechanism was studied by isothermal methods, where plot of equilibrium absorbance versus NPs suspension concentration was fit with two different models: Langmuir and Freundlich. The Langmuir model assumes the formation of a monolayer of adsorbed material on the substrate, with no influence from previously adsorbed species, while the Freundlich model is applicable to systems in which heterogeneous adsorption reactions occur and lead to formation of multilayers. Fig. 3 presents the results of both models; the Freundlich model gave a better fit to the data. Contrary, in the contribution of Alcantara et al. [42], the experimental data fitted better with Langmuir model, showing that deposition condition affects not only kinetic mechanism but also the adsorption isotherm.

FESEM images were taken from films with different numbers of bilayers. Fig. 4 shows the images obtained from films with 1, 8, 16 and 32 bilayers. With 8 bilayers, the substrate was not fully covered by the film; with 16 bilayers the substrate is fully covered being possible to observe a nanostructured and uniform deposit.

The thickness of a 25-bilayer film was obtained by profilometry from a fracture made with a scalpel in the multilayer film. The depth was measured at 60 points along the fracture, and the average thickness is (171 ± 28) nm, corresponding to a bilayer thickness of approximately 7 nm.

3.2. Electrochemical characterization

Although an electrical connection among nanoparticles in different bilayers is possible in films made by layer-by-layer deposition [7], it was necessary to verify if the upper bilayers maintain this electric connection because PAH is an insulator. This verification was carried out with linear voltammetry for films with different numbers of bilayers (Fig. 5).

The charge density was calculated by integrating the current versus time curves; it increases linearly up to 25 bilayers, which means that the electric connection is maintained among the NPs and with the current collector until this number of bilayers. However, increasing the number of bilayers decreases the charge density instead of keeping it constant, which was unexpected. This can be explained from the fact that the upper layers not only do not participate in the electrochemical process, but also act as a barrier to the electrolyte, preventing it from reaching the electroactive portion of the film. With this result, it is possible to define the optimum number of bilayers as 25.

Charge/discharge behavior was studied in two different electrolytes: $LiClO_4$/PC and $LiCF_3SO_3$/$BMMITf_2N$. The anion $CF_3SO_3^-$ is structurally similar to the commonly used Tf_2N^- and was used due its higher ionic conductivity in the mixture with the ionic liquid at the concentration employed in the present study. Fig. 6 presents voltammetric profiles for the first four cycles in both electrolytes.

The voltammogram obtained in the organic solvent-based electrolyte (Fig. 6a) shows well-defined oxidation (at 2.65 V more intense and 2.45 V less intense) and reduction (at 2.55 V more intense and 2.84 V less intense) peaks, which correspond to

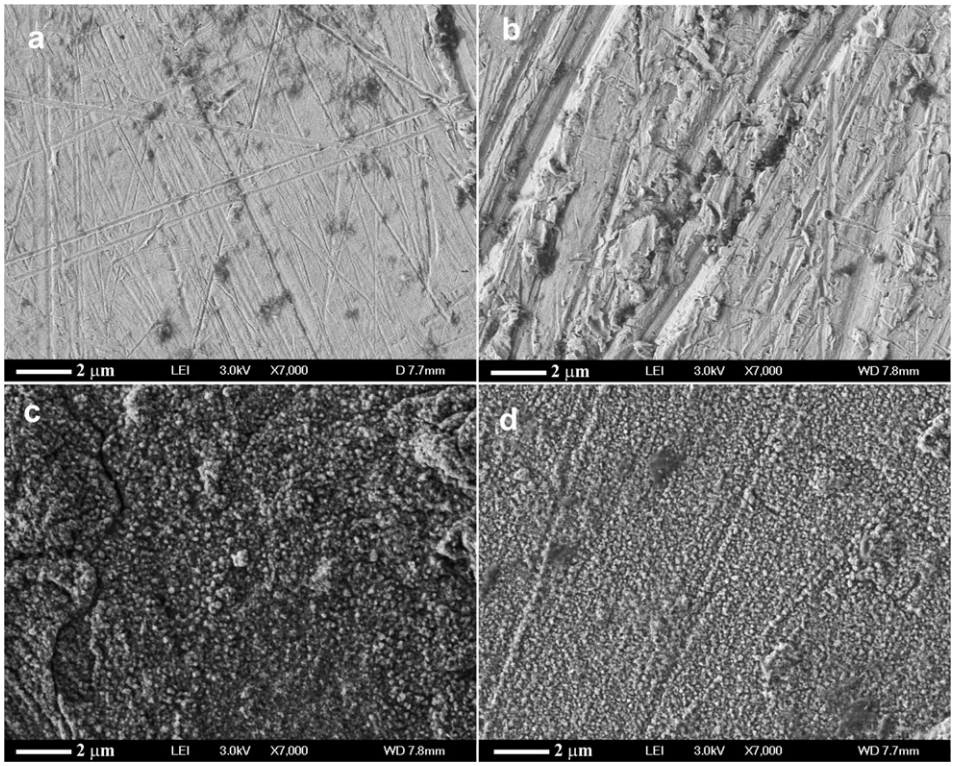

Fig. 4. FESEM images taken from PAH/NPs films deposited over gold substrates with (a) 1, (b) 8, (c) 16 and (d) 32 bilayers.

deintercalation and intercalation of Li^+ into the vanadium oxide structure, respectively. The current intensity decreases with cycling, along with slight shifts of the peaks to less positive potentials. In the ionic liquid-based electrolyte (Fig. 6b), in addition to the peaks observed in the carbonate propylene electrolyte, one reduction peak at 2.94 V is also observed, but only in the first cycle. The peaks are also well defined in the first cycle, however, their enlargement is observed in the subsequent cycles, suggesting loss of crystallinity with successive Li^+ intercalation/deintercalation in the film structure when the ionic liquid is used as the electrolyte. Loss of crystallinity within cycling are well known to happen when high content of Li^+ is inserted into the material structure, which is not the case in the potential range adopted for the present study. However, contrary to usual organic solvent used as electrolytes, ionic liquids are purely composed of ionic species that can also participate in the charge compensation during the oxidation/reduction processes as it was pointed out in reference [7]. As the

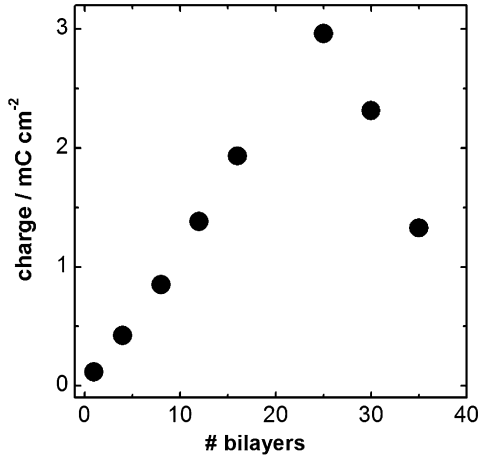

Fig. 5. Charge density calculated from linear voltammograms of films deposited on ITO substrates with different number of bilayers. Scan rate: 2.5 mV s^{-1}; electrolyte: $LiClO_4$ 0.5 mol L^{-1} in PC; counter electrode and reference electrodes: Li sheet; pre-treatment: 2.0 V for 10 min; and range: from 2.0 to 3.6 V.

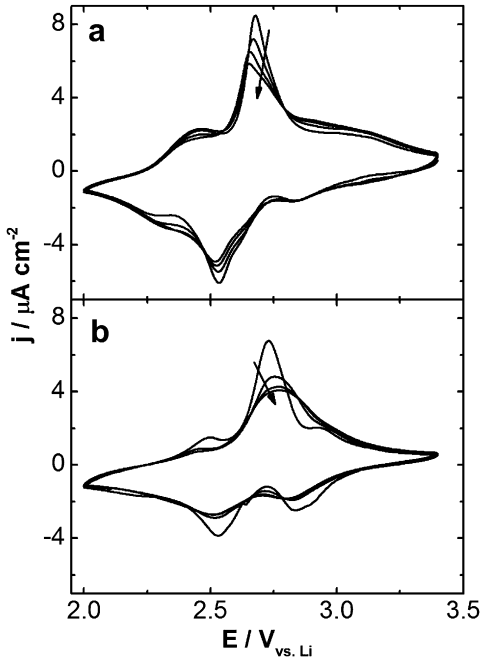

Fig. 6. Cyclic voltammetry profiles of films with 25 bilayers deposited on ITO. Scan rate: 0.1 mV s^{-1}; counter and reference electrodes: Li sheet; pre-treatment: 3.6 V for 10 min; electrolyte: (a) $LiClO_4$ 0.5 mol L^{-1} in PC and (b) $LiCF_3SO_3$ 0.03 mol L^{-1} in $BMMITf_2N$.

ions from ionic liquids are bigger, they can disturb the lattice parameters, causing the loss of crystallinity observed in the experiments.

The subsequent cycles does not cause significant changes, at least up to the 20th cycle. The FESEM images of the films, before and after cycling, show that the morphology is maintained, with no evidence of film dissolution or agglomeration of particles (Fig. 7).

Discharge capacity values were calculated by integrating the current versus time profiles over 20 charge/discharge cycles for both electrolytes. Fig. 8 presents the resulting values as a function of the number of cycles.

Accordingly to the obtained results, for the system containing the organic solvent-based electrolyte, the capacity increases during the first cycles from 280 Ah kg^{-1} to 320 Ah kg^{-1}, but continuous capacity fading is observed over the charge/discharge cycles. However, for the system containing the ionic liquid-based electrolyte, the capacity initially decreases from 245 Ah kg^{-1} to 210 Ah kg^{-1} during the first three cycles, and no further capacity fading is observed during subsequent cycles.

In a recent contribution from Quinzeni et al. [43], thin films of V_2O_5 were prepared by reactive radio frequency magnetron sputtering, a technique that requires a high vacuum and sophisticated equipment. The resulting films, with different thicknesses, were electrochemically characterized in a conventional organic solvent-based electrolyte, and showed promising results. At a similar discharge rate (0.2 C) and greater film thickness (320 nm) than that employed in the present work, the measured initial discharge capacity was approximately 140 mAh g^{-1}. This result was below the value reported here for both the ionic liquid- and organic solvent-based electrolytes.

At the employed potential window, the intercalation of 1 mol of Li^+ per mol of V^{5+} occurs when one considers V_2O_5 [44]. In the bariandite oxide structure, the formal V^{5+}/V^{4+} proportion is 4:1. If one also considers insertion of 1 mol of Li^+ per mol of V^{5+}, the calculated theoretical capacity is 206 Ah kg^{-1}, which means that more than 1 mol of Li^+ per mol of V^{5+} intercalates in both electrolytes at this potential range, i.e., part of vanadium is being reduced to V^{3+}.

Previous work by Le et al. [45] showed that the potential window for intercalation of 1 mol of Li^+ per mol of V^{5+} in vanadium oxide is narrower for the aerogel structure than for xerogels,

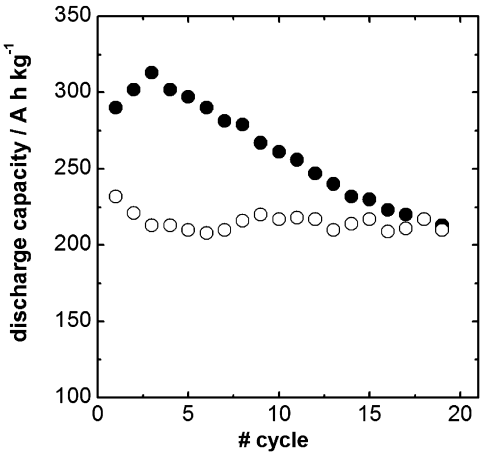

Fig. 8. Discharge capacity calculated from cyclic voltammograms of VO_x films with 25 bilayers on ITO. Scan rate: 0.1 mV s^{-1}; counter and reference electrodes: Li sheet; electrolytes: $LiClO_4$ 0.5 mol L^{-1} in PC (●) and $LiCF_3SO_3$ 0.03 mol L^{-1} in $BMMITf_2N$ (○).

showing that the surface area influences the electrochemical performance not only in terms of amount of material available for Li^+ intercalation but also in its mechanism. A more open structure can allow intercalation of more than 1 mol of Li^+ per mol of transition metal, resulting in higher capacity relative to more compact structures.

Experiments done at different scan rates (not shown) have shown that at rates as high as 1 mV s^{-1} and 10 mV s^{-1}, the discharge capacities are still maintained at 44% and 37% of theoretical value respectively in the propylene carbonate based electrolyte. This result, together with the fact that more than 1 mol of Li^+ per mol of V^{5+} is involved in the charge/discharge process at low scan rate, shows that the oxide structure employed in the present work is open enough to avoid the problems related with rate capability usually present in vanadium oxides structures.

Accordingly to a previous report [46], intercalation of more than 1 mol of Li^+ per mol of V^{5+} causes structural changes and requires more positive potentials for removal of extra intercalated

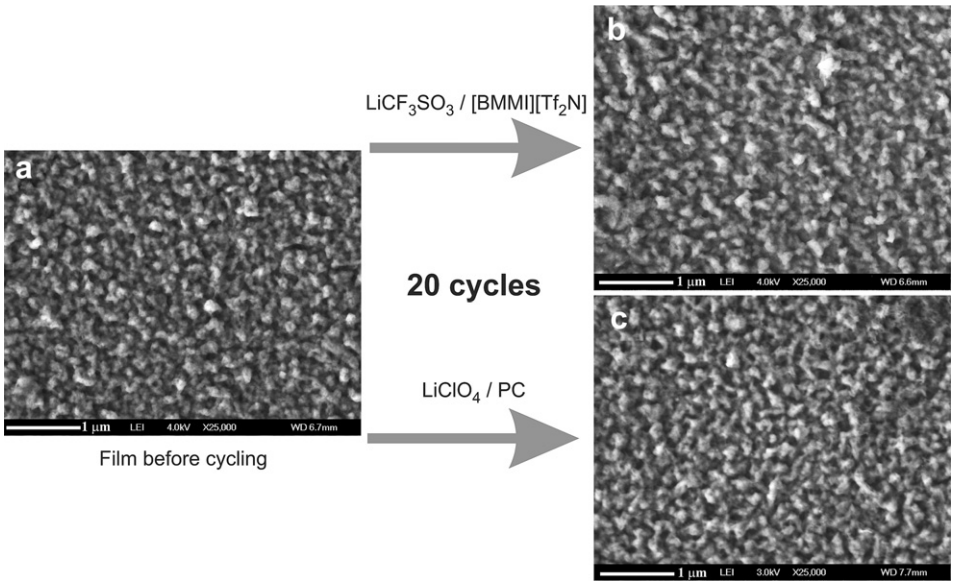

Fig. 7. FESEM images of films with 25 bilayers deposited on ITO (a) before cycling, (b) after 20 voltammetry cycles in $LiCF_3SO_3$ 0.03 mol L^{-1} in $BMMITf_2N$ and (c) after 20 cycles in $LiClO_4$ 0.5 mol L^{-1} in PC. Scan rate: 0.1 mV s^{-1}; and counter and reference electrodes: Li sheet.

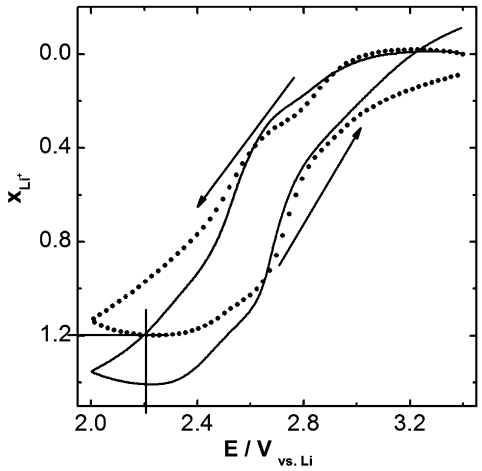

Fig. 9. $x\mathrm{Li}^+$ inserted in NP films as a function of applied potential in the first cyclic voltammetry cycle. Scan rate: 0.1 mV s^{-1}; counter and reference electrodes: Li sheet; electrolytes: $LiClO_4$ 0.5 mol L^{-1} in PC (–) and $LiCF_3SO_3$ 0.03 mol L^{-1} in $BMMITf_2N$ (●).

Li^+, which leads to capacity fading. In the present study, for the system containing the organic solvent-based electrolyte, after initial capacity increase during the first cycles, continuous capacity fading is observed over the charge/discharge cycles. However, for the system containing the ionic liquid-based electrolyte, the capacity initially decreases, but no further capacity fading is observed during subsequent cycles. These results suggest that, in the system containing the organic solvent electrolyte, capacity fading is caused by irreversible Li^+ intercalation once higher amount of the cationic specie is involved in charge compensation process.

Other reasons for the better performance of the system containing the ionic liquid-based electrolyte can be attributed to the decrease in the crystallinity of the electroactive material, which ensures that there is less mechanical stress with successive Li^+ insertion/deintercalation [47] and protects the cathode from discharge capacity loss caused by irreversible structural changes [48]. In fact, the enlargement of voltammetry peaks with cycling is an evidence of loss of crystallinity when the ionic liquid electrolyte was used. Additionally, formation of a more stable SEI in ionic liquids prevents film dissolution, as noted by Dou et al. [33], who observed better performance in terms of discharge capacity of a vanadium oxide composite with polypyrrole in an ionic liquid-based electrolyte. However, in terms of stability over several charge/discharge cycles, the performance of the system described by Dou et al. was better in the organic solvent-based electrolyte.

If one considers that capacity fading is caused by irreversible intercalation of Li^+, the intercalation of extra Li^+ into the structure should be prevented to produce a more stable system in conventional organic solvents, which means that the potential window should be reduced, resulting in lower capacity density. In the first charge/discharge cycle in ionic liquid-based electrolyte, there is intercalation of approximately 1.2 mol of Li^+ per mol of V^{5+}. To maintain the same amount of Li^+ in the charge/discharge process in both electrolytes, the potential window of the system containing the organic solvent should be decreased in 0.2 V as it possible to observe in Fig. 9.

As system performance depends not only on charge capacity but also on the potential window, this reduction would decrease the performance by 25% in terms of energy density. With the ionic liquid-based electrolyte, it is possible to maintain the system stability in a wider potential window, resulting in higher energy density.

4. Conclusions

The construction of nanostructured thin films of $V_{10}O_{24}\cdot 9H_2O$ through layer-by-layer deposition technique has been systematically studied by UV–vis, QCM and linear voltammetry, being possible to optimize the conditions for obtention of the most suitable system.

The obtained film presented good electrochemical performance in both conventional organic solvent- and ionic liquid-based electrolytes, being better, in terms of stability during consecutive charge/discharge cycles, with the ionic material. This result can be attributed to several factors: reduction in the mechanical stress caused by insertion of more than 1 mol of Li^+ per mol of V^{5+} in the film structure, decrease in the crystallinity of the electrode material in the first charge/discharge cycle and/or formation of a more compatible SEI. In summary, results obtained with the system containing the LBL thin film and ionic liquid based electrolyte are promising for microbatteries application.

Acknowledgments

Financial support was provided by Fapesp (2005/59135-6, 2012/02117-0 and 2009/53199-3), INCT in Bioanalytics (FAPESP, Grant 08/57805-2), CNPq, CAPES and NENNAM (Pronex, F. Araucária/CNPq).

References

[1] J. Hassoun, P. Real, B. Scrosati, J. Mater. Chem. 17 (2007) 3668–3677.
[2] C. Julien, A. Gorenstein, Ionics 1 (1995) 193–210.
[3] A. Patil, D.W. Shin, J.-W. Choi, D.-S. Piak, S.-J. Yoon, Mater. Res. Bull. 43 (2008) 1913–1942.
[4] B.L. Ellis, K.T. Lee, L.F. Nazar, Chem. Mater. 22 (2010) 691–714.
[5] Y.G. Xia, Q. Zhang, H.Y. Wang, H. Nakamura, H. Noguchi, M. Yoshio, Electrochim. Acta 52 (2007) 4708–4714.
[6] T.M. Benedetti, V.R. Goncales, D.F.S. Petri, S.I. Cordoba de Torresi, R.M. Torresi, J. Braz. Chem. Soc. 21 (2010) 1704–1709.
[7] T.M. Benedetti, F.F.C. Bazito, E.A. Ponzio, R.M. Torresi, Langmuir 24 (2008) 3602–3610.
[8] Y. Wang, G. Cao, Chem. Mater. 18 (2006) 2787–2804.
[9] E.A. Ponzio, T.M. Benedetti, R.M. Torresi, Electrochim. Acta 52 (2007) 4419–4427.
[10] M. Malta, L.H. Silva, A. Galembeck, M. Korn, Macromol. Rapid Commun. 29 (2008) 1221–1225.
[11] M. Malta, G. Louarn, N. Errien, R.M. Torresi, J. Power Sources 156 (2006) 533–540.
[12] F. Hughenin, R.M. Torresi, J. Phys. Chem. C 112 (2008) 2202–2209.
[13] F. Huguenin, D.S. dos Santos, A. Bassi, F.C. Nart, O.N. Oliveira, Adv. Funct. Mater. 14 (2004) 985–991.
[14] S.H. Choi, J.H. Kim, Y.N. Ko, Y.J. Hong, Y.C. Kang, J. Power Sources 210 (2012) 110–115.
[15] F. Lian, M. Gao, W.H. Qiu, P. Axmann, M. Wohlfahrt-Mehrens, J. Appl. Electrochem. 42 (2012) 409–417.
[16] H. Yu, H. Kim, Y. Wang, P. He, D. Asakura, Y. Nakamura, H. Zhou, Phys. Chem. Chem. Phys. 14 (2012) 6584–6595.
[17] Y. Kim, ACS Appl. Mater. Interfaces 4 (2012) 2329–2333;
W.C. West, J. Soler, B.V. Ratnakumar, J. Power Sources 204 (2012) 200–204.
[18] L. Li, Z. Guo, A. Du, H. Liu, J. Mater. Chem. 22 (2012) 3600–3605.
[19] L. Noerochim, J.-Z. Wang, D. Wexler, M. Rahman, J. Chen, H.-K. Liu, J. Mater. Chem. 22 (2012) 11159–11165.
[20] H. Liu, G. Yang, X. Zhang, P. Gao, L. Wang, J. Fang, J. Pinto, X. Jiang, J. Mater. Chem. 22 (2012) 11039–11047.
[21] X. Chen, E. Pomerantseva, P. Banerjee, K. Gregorczyk, R. Ghodssi, G. Rubloff, Chem. Mater. 24 (2012) 1255–1261.
[22] S. Zhou, X. Yang, Y. Lin, J. Xie, D. Wang, ACS Nano 6 (2012) 919–924.
[23] Y.Q. Qiao, J.P. Tu, X.L. Wang, J. Zhang, Y.X. Yu, C.D. Gu, J. Phys. Chem. C 115 (2011) 25508–25518.
[24] Y. Yang, D. Kim, P. Schmuki, Electrochem. Commun. 13 (2011) 1198–1201.
[25] K. West, B.Z. Christiansen, M.J.L. Ostergard, T. Jacobsen, J. Power Sources 42 (1993) 127–134.
[26] N.A. Galiote, M.N.L. Camargo, R.M. Iost, F. Crespilho, F. Huguenin, Langmuir 27 (2011) 12209–12217.
[27] W.G. Menezes, D.M. Reis, M.M. Oliveira, J.F. Soares, A.J.G. Zarbin, Chem. Phys. Lett. 445 (2007) 293–296.
[28] H. Ohno, Electrochemical Aspects of Ionic Liquids, John Wiley & Sons Inc., USA, 2005 (chapter 1).

[29] A. Fernicola, B. Scrosati, H. Ohno, Ionics 12 (2006) 95–102.
[30] M. Armand, F. Endres, D.R. MacFarlane, H. Ohno, B. Scrosati, Nat. Mater. 8 (2009) 621–629.
[31] W.G. Menezes, D.M. Reis, T.M. Benedetti, M.M. Oliveira, J.F. Soares, R.M. Torresi, A.J.G. Zarbin, J. Colloid Interface Sci. 337 (2009) 586–593.
[32] S.Y. Chew, J. Sun, J. Wang, H. Liu, M. Forsyth, D.R. MacFarlane, Electrochim. Acta 53 (2008) 6460–6463.
[33] S.-L. Chou, J.-Z. Wang, J.-Z. Sun, D. Wexler, M. Forsyth, H.-K. Liu, D.R. MacFarlane, S.-X. Dou, Chem. Mater. 20 (2008) 7044–7051.
[34] F.F.C. Bazito, Y. Kawano, R.M. Torresi, Electrochim. Acta 52 (2007) 6427–6437.
[35] C. Gabrielli, M. Keddam, R.M. Torresi, J. Electrochem. Soc. 138 (1991) 2657–2660.
[36] G.G. Nunes, G.R. Friedermann, J.L.B. Dos Santos, M.H. Herbst, N.V. Vugman, P.B. Hitchcock, G.J. Leigh, E.L. Sa, C.J. Da Cunha, J.F. Soares, Inorg. Chem. Commun. 8 (2005) 83.
[37] G. Sauerbrey, Z. Phys. 155 (1959) 206–222.
[38] G. Decher, Science 277 (1997) 1233–1237.
[39] Y.S. Ho, G. McKay, Process. Biochem. 34 (1999) 451–465.
[40] F.-C. Wu, R.-L. Tseng, S.-C. Huang, R.-S. Juang, Chem. Eng. J. 151 (2009) 1–9.
[41] M. Toor, B. Jin, Chem. Eng. J. 187 (2012) 79–88.
[42] G.B. Alcantara, L.G. Paterno, A.S. Afonso, R.C. Faria, M.A. Pereira-da-Silva, P.C. Morais, M.A.G. Soler, Phys. Chem. Chem. Phys. 13 (2011) 21233–21242.
[43] I. Quinzeni, S. Ferrari, E. Quartarone, P. Mustarelli, J. Power Sources 196 (2011) 10228–10233.
[44] C. Delmas, H. Cognac-Auradou, J.M. Cocciantelli, M. Ménétrier, J.P. Doumerc, Solid State Ionics 69 (1994) 257–264.
[45] D.B. Le, S. Passerini, A.L. Tipton, B.B. Owens, W.H. Smyrl, J. Electrochem. Soc. 142 (1995) L102–L103.
[46] C. Delmas, S. Brethes, M. Ménétrier, J. Power Sources 34 (1991) 113–118.
[47] M. Nabavi, C. Sanchez, F. Taulenne, J. Liavge, Solid State Ionics 28–30 (1988) 1183–1186.
[48] K. West, B.Z. Christiansen, S.V. Skaarup, Solid State Ionics 57 (1992) 41–47.